Title Page

Title: Cross-Species Insight into Abdominal Aortic Aneurysm: Deciphering the Myeloid Code in Human and Mouse Models

Short title: Cross-Species Analysis of AAA Myeloid Cells

Authors: Xiaoxu Zhang[1#], Xu Guo[1#], Jamol Uzokov[2], Han Jiang[3], Azad Hussain[4], Deying Jiang[5], Yuemeng Li[5], Chen Chen[6], Yanshuo Han[1,5*], and Jian Zhang[3*].

1. School of Life and Pharmaceutical Sciences, Dalian University of Technology, Panjin, 124001 China.

2. Republican Specialized Scientific Practical Medical Center of Therapy and Medical Rehabilitation, Tashkent, Uzbekistan 4 Osiyo Tashkent, Uzbekistan

3. Department of Vascular Surgery, The First Hospital of China Medical University, Shenyang, 110001, China.

4. Department of Mathematics, University of Gujrat, Gujrat, 50700, Pakistan.

5. Department of Vascular Surgery, Central Hospital of Dalian University of Technology, Dalian, 116024, China.

6. School of Biomedical Sciences, University of Queensland, Brisbane, QLD, Australia.

Corresponding authors:

0

 # Contributed equally.

The category of the manuscript: Original Articles

Total word count of the manuscript:8,428

Abstract

Using single-cell sequencing, we analyzed over 130,000 cells from human AAA samples and mouse models, performing functional and genetic classification of myeloid macrophages. We identified eight conserved macrophage subsets shared between humans and mice, underscoring the robustness of mouse models in mimicking human disease mechanisms and revealing potential for AAA translational research. Advanced tools like Monocle 3 and CellChat helped us explore immunoregulatory functions, track developmental trajectories, and map cell communication networks, discovering high cross-species expression of SPP1/CD44. Additionally, SCENIC identified common transcriptional regulators in the AAA environment, validating potential regulatory transcription factor targets. This study highlights the critical role of myeloid cells in AAA pathogenesis, confirms the potential of mouse models for therapeutic interventions, and uncovers significant crosstalk between transcription factors, deepening the understanding of AAA pathology and identifying potential therapeutic targets.

Keywords: Abdominal aortic aneurysm; Myeloid cells; Single-cell RNA sequencing; Cross-species analysis; Tissue-resident macrophages; Therapeutic targets for AAA.

1. Introduction

Abdominal aortic aneurysm (AAA) constitutes a formidable vascular pathology characterized by a perilous dilation of the abdominal aorta, with potentially fatal outcomes. The definition of abdominal aortic aneurysm is established when the diameter of the aorta exceeds 1.5 times its normal size. As the aneurysm progresses, the condition is considered highly critical. The increased intravascular pressure and enlarged vessel diameter elevate the risk of aortic wall rupture, leading to catastrophic internal bleeding and subsequently, an elevated mortality rate(Golledge, 2019; Sakalihasan et al., 2018). The genesis of AAA involves a multifaceted interaction of genetic, environmental, and lifestyle determinants, yet the detailed molecular underpinnings of its onset remain obscure(Sakalihasan et al., 2005). Complicating its clinical management, AAA often progresses asymptomatically, thus hindering early detection and continuous surveillance(Nordon et al., 2011).

At the core of AAA pathogenesis lies the instrumental role of both adaptive and innate immune responses, especially their contributions to vascular inflammation and structural compromise within the vessel wall(Gao et al., 2023). Myeloid lineage cells, including a spectrum of macrophages and monocytes, play a pivotal role in exacerbating vascular inflammation, promoting extracellular matrix degradation(Yang et al., 2014), and facilitating vessel wall weakening and dilation through the emission of pro-inflammatory cytokines, proteolytic enzymes, and various mediators(Raffort et al., 2017). A sophisticated comprehension of the distinct mononuclear phagocyte subsets and their specific functional states under physiological and inflammatory

conditions is crucial for understanding their contribution to both health and disease states. Traditionally, the M1/M2 paradigm was utilized to classify macrophage activation states(Murray et al., 2014; Orecchioni et al., 2019); However, the advent of single-cell sequencing technologies has challenged these classifications, rendering conventional markers such as CD206 and CD86 insufficient for precise differentiation(Nahrendorf and Swirski, 2016; Shi et al., 2022). Consequently, the accurate identification and categorization of cell-type-specific subsets and states within single-cell transcriptomic analyses present a considerable challenge, necessitating an enhanced classification scheme for mononuclear phagocytes and their associated markers in the context of AAA(Nalio Ramos et al., 2022).

Mouse models are indispensable in biomedical research, attributed to their genetic and physiological similarities to humans and the facility of genetic manipulation(Rateri et al., 2011). Nonetheless, the translation of findings from mouse models to human pathology requires meticulous attention to interspecies variances(Ishibashi et al., 2004; Trollope et al., 2011). In the context of AAA, a detailed delineation of mononuclear phagocyte subsets and their activation states in both health and disease is essential for an in-depth exploration of their functional contributions(Yang et al., 2014).

This investigation conducts a comparative analysis of monocyte and macrophage subpopulations from human and mouse origins, with a focus on shared myeloid system subsets. Our results unveil conserved gene expression and transcriptional profiles among myeloid cells, particularly macrophages, across species. We have delineated cross-species markers for the identification of myeloid cell subpopulations.

Through this cross-species analysis, we underscore the genetic and transcriptional congruencies between mouse models and human AAA, thereby providing a robust foundation for the advancement of our comprehension and therapeutic approaches for AAA.

2. Methods

2.1 Human Samples and Cell Preparation for scRNA-seq

In this investigation, seven patients diagnosed with abdominal aortic aneurysm (AAA) and six healthy controls were sequentially recruited (**Supplementary Table S1**). AAA patients underwent aneurysmal open surgical repair at the First Hospital of China Medical University, where tissue specimens and relevant clinical data were systematically gathered. Individuals presenting with Ehlers-Danlos syndrome, Marfan syndrome, other identifiable vascular or connective tissue disorders, cancer, infectious diseases, or any autoimmune conditions were rigorously excluded from participation. For single-cell RNA sequencing (scRNA-seq) purposes, AAA and control tissue samples were preserved in a proprietary tissue storage solution obtained from SeekGene BioSciences Co., Ltd., Beijing, China, and were transported at 4°C to the SeekGene BioSciences laboratory.

Post-collection, tissues were promptly rinsed with ice-cold RPMI1640 medium and dissociated utilizing the Multi-Tissue Dissociation Kit 2 (Miltenyi Biotec, Germany) as per the manufacturer's protocol. Cellular viability and count were assessed using a Countstar Rigel S2 Fluorescence Cell Analyzer with acridine orange/propidium iodide (AO/PI) staining, following erythrocyte removal (Miltenyi Biotec) and the clearance of any detritus or non-viable cells as deemed necessary. Subsequently, viable cells were washed twice with RPMI1640 and resuspended in 1 × PBS containing 0.04% bovine serum albumin at a concentration of 1×10^6 cells/ml.

2.2 ScRNA-seq Library Construction and Sequencing

The scRNA-seq libraries were constructed employing the SeekGene SeekOne® MM Single Cell 3' Library Preparation Kit. Initially, a specified number of cells were placed into the SeekOne® MM chip's flow channel, equipped with 170,000 microwells. After a period for cell settling, unattached cells were removed. Cell Barcoded Magnetic Beads (CBBs) were then added to the flow channel, and with a magnetic field, allocated precisely into the microwells. The cells were lysed on the chip, releasing RNA that was captured by the adjacent CBBs. Reverse transcription at 37°C for 30 minutes allowed for cDNA synthesis, incorporating cell-specific barcodes. Exonuclease I removed residual primers from the CBBs.

Following this, barcoded cDNA underwent hybridization with a random primer for second DNA strand synthesis, embedding the cell barcode at the 3’ end. The DNA was then purified, amplified via PCR, and refined using SPRI beads. Full-length sequencing adapters and sample indices were added through indexed PCR. The libraries were quantified via quantitative PCR (KAPA Biosystems KK4824) and sequenced on either the Illumina NovaSeq 6000 or the DNBSEQ-T7 platform, as required by our analysis.

2.3 Single-cell RNA sequencing data processing

2.3.1 Human Single-Cell Data Integration and Quality Control

In the analysis of human samples, the single-cell RNA-seq data from seven AAA samples and six control samples were processed separately to maintain the integrity

of each condition's dataset. For the AAA dataset, cell matrix files were imported into R using the CreateSeuratObject function in Seurat (version 4.4.0)(Stuart et al., 2019).Cells expressing fewer than 200 genes or more than 6,600 genes were excluded to ensure data quality. Additionally, cells with over 25% of transcripts from mitochondrial genes were deemed potentially apoptotic and excluded. For the control dataset, similar quality control measures were applied, with the exception that cells expressing more than 5,500 genes were excluded, aligning with the distinct characteristics of these samples. After quality control and exclusion of low-quality cells, batch effects within each dataset were corrected using Harmony(Korsunsky et al., 2019). Doublets were identified and removed using DoubletFinder(McGinnis et al., 2018) with default settings. This preprocessing resulted in 42,287 cells from the AAA dataset and 35,785 cells from the control dataset, both of which were used for subsequent analyses.

2.3.2 Mouse Single-Cell Data Integration and Quality Control

In this study, a comprehensive single-cell transcriptomic analysis was conducted on mouse AAA and control samples by integrating data from multiple public datasets. AAA (**Supplementary Table S2**) and control datasets (**Supplementary Table S3**) were processed separately, with AAA samples coming from three datasets (GSE152583, GSE186865, GSE164678, and GSE221789) and control samples from three datasets (GSE221789, GSE164678, and GSE244246). The modeling methods for the construction of abdominal aortic aneurysms in mice vary. Angiotensin II perfusion was

used in GSE186865 and GSE221789, while elastase-induced mouse models were employed in GSE152583. Additionally, in GSM5016937, $CaCl_2$ perfusion was used to induce abdominal aortic aneurysms. All the data we crawled were from mice that were induced to develop abdominal aortic aneurysms. The single-cell expression matrices from these samples were merged within their respective groups, and a common set of genes was identified for further analysis. Using Seurat, cells were filtered out if they expressed fewer than 200 or more than 6,000 genes (6,500 for control samples) or if over 25% of their transcripts were of mitochondrial origin, indicative of potential apoptosis. Batch effects and doublets within each group were addressed using Harmony and DoubletFinder, respectively. The quality control and preprocessing steps yielded 20,320 cells from AAA samples and 29,224 cells from control samples for downstream analysis.

2.4 Single-Cell Data Dimensionality Reduction, Clustering, and Annotation

Initially, datasets were normalized employing the NormalizeData function, setting the stage for the selection of the top 2,000 variable genes based on the variance stabilizing transformation (VST) method. Subsequently, the data was scaled to ensure that each gene's expression measurements were centered around a mean of zero and standardized with a variance of one. Following scaling, we embarked on dimensionality reduction through principal component analysis (PCA). Clustering was performed with a resolution parameter of 0.8 for the majority of datasets, with the exception of the human control group, which was processed at a resolution of 1.2. This

differentiation in resolution parameters was strategically employed to accommodate the unique characteristics of the human control group, enabling a more nuanced identification of cell populations. Finally, the dimensionality of each dataset was further reduced using Uniform Manifold Approximation and Projection (UMAP).

Subsequently, we leveraged the FindAllMarkers function in Seurat to pinpoint distinctive markers for each cell cluster. Concurrently, SingleR(Aran et al., 2019), an automated annotation tool, was deployed to further refine cell cluster characterization. This dual approach facilitated a robust and comprehensive identification of major cell populations. By integrating well-established marker genes sourced from an extensive review of the literature with the cluster-specific markers identified through FindAllMarkers, we were able to achieve a nuanced and accurate determination of cell identities.

2.5 Clustering and Annotation of Human Myeloid Cells

To achieve a holistic integration of human and mouse AAA myeloid cell data, we first transformed mouse genes to their corresponding human orthologs, leading to an 11.2% decrease in gene count. This step was essential for aligning genetic terminologies and ensuring accurate interspecies comparisons. We then identified 11,611 genes at the intersection of the transformed mouse and human datasets, harmonizing the gene count across both species. For the 14 AAA samples (7 human and 7 mouse), we individually processed each through Seurat, utilizing an anchor-finding process with 1,000 genes to aid in the integration, and merged them using the IntegrateData

function. This approach preserved the biological integrity of the datasets across species. After integration, we applied PCA and UMAP clustering for dimensionality reduction, similar to previous procedures, culminating in a comprehensive dataset of integrated human and mouse AAA myeloid cells. Furthermore, we refined the annotation of myeloid cells from both species using SingleR and extensive literature review. This detailed annotation process, which will be elaborated upon in the results section, enhanced our understanding of the nuanced roles of these cells.

2.6 Integration of Human and Mouse Myeloid Cell Single-Cell Data

In the integration of human and mouse AAA myeloid cell data, we first converted mouse genes to their human orthologs, leading to a 11.3% reduction in mouse gene count, a necessary step for unifying genetic terminology across species. This process yielded a shared set of 11,611 genes. We then harmonized gene counts across the 14 AAA samples，by processing each through Seurat, using an anchor-finding process with 1,000 genes for integration via the IntegrateData function. This approach ensured a cohesive dataset that reflects true biological signals from both species. Finally, we employed PCA for dimensionality reduction and UMAP for clustering, producing an integrated human-mouse AAA myeloid cell dataset that encapsulates the complex interplay of genetic expressions across species.

2.7 Pseudotime Analysis Reveals Myeloid Cell Developmental Trajectories in Humans and Mouse

We embarked on a pseudotime analysis using Monocle3(Cao et al., 2019; Qiu et al., 2017a; Qiu et al., 2017b; Trapnell et al., 2014) for three distinct datasets: human AAA myeloid cells, mouse AAA myeloid cells, and an integrated dataset of human and mouse AAA myeloid cells. Each dataset underwent a separate analysis, enabling the detailed visualization of myeloid lineage developmental trajectories on their respective UMAP plots. The integrated dataset allowed us to examine the expression patterns of markers shared by humans and mouse, such as those indicative of macrophages, dendritic cells (DCs), and monocytes, across pseudotime.

2.8 Analyzing Transcription Factor Activity in AAA Myeloid Cells Using SCENIC

In our investigation, we utilized the SCENIC(Aibar et al., 2017) protocol to perform transcription factor (TF) analysis on both human and mouse AAA myeloid cell datasets. SCENIC, an innovative computational approach, enables the discovery of gene regulatory networks within single-cell RNA-seq data, revealing active transcription factors and their regulatory influence across myeloid cell populations of each species. To visualize the regulatory landscapes, we employed the R package pheatmap, creating heatmaps that display the averaged and scaled activity scores (AUCell values)(Clarke et al., 2021) of crucial transcription factors shared by humans and mouse, reflecting their regulatory potential across different myeloid cell types. Furthermore, we generated UMAP plots to illustrate the spatial distribution of these key transcription factors within the myeloid cell landscape.

2.9 Dissecting Cell-Cell Communication in AAA Using CellChat

In our study, we utilized the CellChat(Jin et al., 2021) tool to analyze cell-cell communication differences within and between myeloid cell populations in human AAA and control groups, as well as in corresponding mouse groups.Our comparative analysis focused on intra-myeloid cell communication, as well as interactions between myeloid cell subtypes and other cell types, including fibroblasts, B cells, and T cells.

2.10 Enrichment Analysis

We conducted enrichment analyses on marker genes identified for various myeloid cell subtypes within both human and mouse datasets. Utilizing the FindMarkers function, we determined the distinct marker genes characterizing each myeloid cell subtype. These marker genes were then converted into their respective ENTREZ IDs to facilitate the enrichment process. The R package clusterProfiler(Yu et al., 2012) was employed to perform the enrichment analysis, enabling us to understand the biological pathways and processes that these markers are involved in. For the visualization of our enrichment analysis results, we used the ggplot2 package, providing a comprehensive and clear representation of the enriched biological terms associated with each myeloid cell subtype's marker genes.

2.11 Western blot analysis

The cells were lysed using RIPA buffer (Solaibao, China) in a 100:1 ratio with PMSF (Solaibao, China) and to extract protein samples. Protein concentration was

determined using BCA protein assay kit (Bioss, China). Sample preparation and Western blot analysis were performed using antibodies against the following proteins: SPP1,CD44,STAT1,NFKB1(P50) (Wanleibio, China) and GAPDH (Sangon Biotech, China); HRP conjugated secondary antibody (Beyotime, China).

2.12 Immunohistochemistry (IHC) assay

Immunohistochemistry on human tumor samples was performed using a 1:100 dilution of anti-SPP1 (rabbit polyclonal, WL02378), a 1:100 dilution of anti-CD44(rabbit polyclonal, WL03531) , 1:100 dilution of anti-p50 (rabbit polyclonal, WL01917), a 1:100 dilution of anti-STAT1(rabbit polyclonal, WL02273), diluted in Ventana antibody diluent (Roche Tissue Diagnostics, 251–018) and detected using the UltraView DAB (Roche Tissue Diagnostics, 760–500) and BOND Refine Polymer DAB (Leica Biosystems, DS9800) detection kits, respectively. Each target was evaluated using. Using the IHC_Toolbox plugin in ImageJ for immunohistochemical analysis, AOD values are used for semi-quantitative tissue-specific expression. The larger the AOD value, the greater the specific staining area.

2.13 Statistical Analysis

Statistical analysis was performed using GraphPad Prism (8.0). Experimental data were presented as the mean ± standard deviation. Based on data distribution and variance homogeneity, data were compared between groups using the t-test, Welch's t-test, or Mann-Whitney U-test as appropriate.

The paired t-test and Wilcoxon paired t-test were used to compare and analyze the difference in IHC variables between AAA and normal tissues. Pearson or Spearman correlation analysis was performed to evaluate correlations between quantitative variables, depending on whether the data showed normal distribution. We considered two-tailed P values of less than 0.05 statistically significant. * $P < 0.05$, ** $P < 0.01$, *** $P < 0.001$, **** $P < 0.0001$.

3 Results

3.1 scRNA-seq profiling the heterogeneity of cells expression of abdominal aorta

Our research aimed to elucidate the diversity inherent in human cellular compositions. We collected fresh abdominal aortic aneurysm (AAA) tissues, including seven samples from AAA patients and six from healthy controls. The single-cell transcriptomic analyses yielded datasets of 42,287 and 39,445 cells for AAA and control samples, respectively. Additionally, AAA and control samples from mouse were retrieved from the Gene Expression Omnibus database, adhering to selection criteria of 200 < nfeature < 6000 and excluding cells with mitochondrial gene content (mt) > 25%. To reconcile batch effects across disparate datasets and ensure significant sample congruity, we employed the Harmony algorithm, followed by normalization and principal component analysis for dimensionality reduction (**Supplementary material, Figure S1B**). Utilizing established markers, we characterized nine subpopulations within human arterial tissues and seven within mouse arterial tissues affected by AAA

(**Figure 1A** and **Figure 1B**).

Our study identified diverse populations of T cells (human: CD3D, CD3E, CD3G; mouse: Cd3e, Cd4, Cd3g) and B lymphocytes (human: CD79A, MZB1, MS4A1; mouse: Cd79a, Cd79b, Ly6d), along with several types of parietal cells: smooth muscle cells (SMC) (human: MYH11, ACTA2, MYL9; mouse: Acta2, Myh11, Cnn1), fibroblasts (human: DCN, COL1A1, COL1A2; mouse: Pdgfra, Col1a1, Lum), endothelial cells (human: PECAM1, PLVAP, PTPRB; mouse: Cdh5, Pecam1, Tie1), in addition to proliferating cells (human: MKI67, TOP2A, CDC20; mouse: Mki67, Top2a, Cdc20). Notably, the myeloid lineage was identified as the most prevalently distributed cell type. We pinpointed cells exhibiting markers characteristic of the myeloid lineage in humans (CD14, CD68, LYZ) and mouse (Adgre1, Cd68, Cd14)(Ouyang et al., 2024; Yu et al., 2022; Zhao et al., 2021)(**Figure 1C**), (**Supplementary material, Figure S1A** and **Figure S1B**). In addition, we also explored Plasmacytoid DC (GZMB, PLAC 8, IRF 4), Plasma cell (IGHGP, FKBP11, XBP1) in human tissues, which revealed the abundance of the samples.

While cell type abundance appeared consistent, discerning differences between control and disease states remains challenging. Despite the heterogeneity among patient samples, scRNA-seq data analysis enabled us to deduce a consistent trend post-AAA development in both humans and mouse: a decrease in SMC content and an increase in fibroblast proportion, indicative of pathological alterations. Additionally, an increase in immune-related cells, including T, B cells, and myeloid cells, was significant compared to control groups(Davis et al., 2022; Sawada et al.,

2021)(**Supplementary material, Figure S1C**). In view of the high abundance and known role of myeloid cells in abdominal aortic aneurysm, we studied different species of myeloid cells and their interactions with lymphocytes, and carefully explored their commonalities and differences to provide genetic information (**Figure 1D**).

3.2 Macrophage subsets in human abdominal aorta

We focus on the changes between myeloid lines and further reduce the dimensionality of human myeloid cells based on characteristic markers. Within AAA patients, we classified macrophages into common categories based on functional characteristics as inflammatory macrophages (CCL3, CCL4, FOS, RGS1, CXCL2, IL1B), tissue-resident macrophages (TRM) (LYVE1, CD163, SEPP1, FOLR2, F13A1, MRC1), and foamy macrophages (TREM2, CD9, GPNMB, SPP1, CTSL, ACP5). According to Bian et al, TRMs can often be identified by varying expressions of CD209(Bian et al., 2020); however, our dataset did not reflect this variability, instead showing uniform high expression. Herein, we defined TRM cells based on the expression of FOLR2(Nalio Ramos et al., 2022), designating them as TRM/FOLR2^{hi}-Mø (F13A1, FOLR2, F13A1, MRC1, LGMN, LYVE1). As for inflammatory macrophages, we categorized them into two types based on gene expression traits. One type, ProInf-Mø (CXCL2, IL1B, CXCL8, TREM1, FN1), exhibited high expression of IL-1b interleukin and genes related to inflammation(Eming et al., 2017). The other type, Inf-Mø (CCL3, CCL4, FOS, HSPA1B, RGS1, IER2), showed high expression of heat shock proteins and chemotactic factors (CCL3, CCL4). Recent studies in the literature have highlighted

some macrophage subsets characteristically expressing Type I interferon response genes and MHCII encoding genes, referred to as IFNIC macrophages (ISG15, IFI6, MX1, CXCL10, IFIT1) (**Figure 2A** and **Figure 2B**). Additionally, we observed that foamy macrophages could be divided into Foamy/SPP1^{hi}-Mø (SPP1, GPNMB, CSTB, APOC1, CTSB), expressing high levels of SPP1 and characteristic foamy genes, and Foamy/ TREM2^{hi}-Mø (TREM2, C1QB, CD14, MTATP6P1, CYBA), expressing high levels of TREM2, a unidirectional transmembrane immune receptor in myeloid cells, with other subsets showing a high expression of the osteopontin gene SPP1 (**Figure 2C** and **Figure 2D**). Further, we collectively grouped myeloid cells into 10 groups, each expressing their respective specific marker (**Figure 2C and Figure 2H**).

The distribution characteristics of these cell types within AAA and diseased groups also merit investigation. Through the evaluation of cell type distribution in scRNA-seq, we concluded that inflammatory macrophages and lipid metabolism-related foamy macrophages are significantly more prevalent in AAA disease than in normal groups (**Figure 2E**). Despite some heterogeneity across samples, the overall trend remained consistent, suggesting that AAA may indeed lead to inflammation and lipid metabolism abnormalities. However, due to the limited sample size, this conclusion is subject to statistical limitations (**Supplementary material, Figure S2A and Figure S2C**).

To mitigate potential stress interferences arising from tissue digestion during sequencing, we explored the expression of stress-induced genes (IEG, LRG, SRF), finding these genes predominantly distributed among inflammatory macrophages. Moreover, pseudotime analysis of human myeloid cells facilitated a better

understanding of temporal developmental changes within the myeloid lineage. Pseudotemporal analysis indicated that monocytes, at the initiation point in time, differentiate into two cell fates. One fate demonstrated monocyte transition into resident cell branches, while the other depicted a division into pro-inflammatory and foamy cell destinies (**Figure 2F**).

We have also utilized several genes that play crucial roles in the disease process and named them accordingly. These include ACP5, which regulates repair and regeneration; Genes involved in immune regulation include those related to inflammation (SPP1), tumor necrosis factor (TNF), immune cell signaling (VSIG4), as well as chemokine-related genes such as CCL3L1 and CCR7 and ERG1, which participates in transcriptional regulation (**Figure 2G and Figure 2I**). Similarly, we can see the trend of high expression of genes in different celltypes between human disease groups and normal tissues shown in the heatmap. (**Figure 2H and Figure 2J**) Notably, we observed a reciprocal correspondence between the genotyping approach based on specific genes and the functional annotation of subpopulations (for instance, immune modulation genes are enriched in regions associated with inflammatory macrophages). This mutually supportive relationship enhances our understanding of the complex cellular interactions and regulatory mechanisms underlying the disease process.

3.3 Analysis of Arterial Macrophage Subpopulations in Mouse

To comprehensively analyze the characteristics of mouse arterial macrophages, we

crawled 6,521 single-cell sequencing datasets from AAA samples and 1,619 datasets from normal vascular samples from the GEO database for further analysis and comparison. Each dataset exhibited a certain degree of heterogeneity (**Figure 3A** and **Figure 3B**) (**Supplementary material, Figure S4A, S4B** and **Figure S5A, S5B**). Myeloid cells were identified based on the expression of Cd14, Adgre1, and Cd68 markers. Subsequently, these cells underwent dimensional reduction with a filtering criterion set at a resolution of 0.8, following the methodology outlined by Zernecke et al(Zernecke et al., 2023). This process led to the identification of three principal groups of mouse macrophages: inflammatory macrophages, foamy macrophages, and tissue-resident macrophages. Our findings regarding the classification of mouse myeloid cells closely aligned with those observed in human samples. Additionally, we identified a cluster of subgroups named TRM, characterized by the high expression of CD209-related genes. Likewise, based on specific markers, we identified the subgroups Foamy/Spp1^{hi}-Mø and Foamy/Trem2^{hi}-Mø in mouse, noted for their high expression of genes related to lipid metabolism, specifically Trem2 and Spp1(Zernecke et al., 2023; Zhang et al., 2023)(**Figure 3C** and **Figure 3D)**. Moreover, as reported in the literature by Han et al., we identified a distinct cluster known as Cavity macrophages, which, unlike in human tissues, are more readily observable in mouse(Han et al., 2024) (**Figure 3A** and **Figure 3C**).

In terms of cell type abundance, there was a conservative increase in the same groups when compared to the control group. In the context of abdominal aortic aneurysms, there was a significant increase in foamy macrophages and a consistent trend in

inflammation-related macrophages (**Supplementary material, Figure S4C** and **Figure S5C**), while the number of TRMs was relatively decreased, mirroring the trends observed in humans (**Figure 3E**) which express specific markers (**Figure 3H** and **Figure 3J**).

Pseudotime analysis revealed that the developmental trajectory of cells is similar to that seen in humans, including the segregation of DC cells from macrophages. Foamy macrophages, appearing at the terminal branch, showcased distinct gene expression patterns indicative of their developmental stage. This suggests a degree of conservation in myeloid development between mouse and humans (**Figure 3F**).

In the sample distribution, we observed an increasing trend of Foamy-Mø in AAAs (**Figure 3E and Figure 3G**). In contrast, TRMs are predominant in normal mouse arteries (**Figure 3I**). Correspondingly, genes such as SPP1 and CCL chemokines, which are characteristic of these subtypes, also show high expression trends in the respective subtypes on the heatmap, strongly supporting our classification results (**Figure 3H and Figure 3J**).

3.4 Integration of Human and Mouse Myeloid Cell Exploration

To investigate the disparities and similarities between humans and mouse in the context of AAA, we initially integrated human and mouse scRNA-seq datasets, isolating specific macrophage myeloid cell lines based on distinct markers. For gene tag conversion between species, we utilized the biologically relevant BioMart-Ensembl database, noting that not all mouse genes have direct human homologs and were thus

463 excluded from our analysis. Following dimensionality reduction and batch effect
464 correction, cluster analysis yielded 10 distinct clusters (**Figure 3A** and **Figure 3B**).
465 Our findings indicate a substantial overlap between human and mouse myeloid cell
466 lines, although the distribution of each subtype varies (**Figure 3C**). Predominantly, in
467 the context of AAA, an increase in inflammatory and foamy macrophages was
468 observed in both species compared to controls, with humans showing a higher
469 propensity for inflammatory macrophages and mouse displaying an increased
470 presence of foamy macrophages. Notably, mouse demonstrated a significant rise in
471 $Trem2^{+}$ foamy macrophages, whereas humans exhibited a greater increase in $SPP1^{+}$
472 macrophages (**Figure 3D**).
473 Furthermore, upon classifying the amalgamated data, we delineated common
474 subgroups across species expressing shared markers, for instance: (I) re-Mono
475 (S100A8, VCAN, SOD2, SELL, G0S2,S MT1G); (II) re-Foamy/$TREM2^{hi}$-Mø (C1QB,
476 C1QC, CTSD, APOC1, GPNMB, TREM2); (III) re-Foamy/$SPP1^{hi}$-Mø (SPP1, GPNMB,
477 CSTD, SDC2, FABP4, ACP5); (IV) re-cDc1 (LGALS2, SLAMF7, PPA1, TAP1,
478 CLEC9A, IRF8); (V) re-cDc2 (CLEC10A, DUSP2, GPR183, LGASLS2, NR4A2,
479 IL1R2); (VI) re-ProInf-Mø (CXCL8, TREM1, CXCL2, IL1B, EREG, C1QC);(VII) re-
480 IFNIC-Mø (IFI6, ISG15, MX1, IFIT2, OAS3, XAF1); (VIII) re-TRM-Mø (SEPP1,
481 MACRO, FLOR2, CD163, F13A1, SLC40A1); (IX) re-Inf-Mø (CCL3, HLA-DRB1,
482 HSPA1A, CCL4, EGR1).
483 To systematically compare myeloid cells between humans and mouse, we explored
484 both similarities and heterogeneities. The UMAP plots revealed that subpopulation

markers are similarly distributed across species, with each cluster containing cells from both humans and mouse, closely mirroring each other in spatial distribution. Additionally, the examination of cell type-specific gene expressions across species indicated that cells of the same type exhibit similar gene expression profiles, although some variances in expression levels exist. This resemblance extends to the development of myeloid cells, with cDC1 and cDC2 showing distinct gene expression patterns compared to other macrophages, yet sharing developmental characteristics between mouse and humans (**Figure 3E**).

Employing the FindMarkers function for subgroups common to both humans and mouse, we retained overlapping components and conducted enrichment analysis. GO enrichment analysis for IFNIC-Mø revealed high enrichment in MHC-related pathways across species, with interferon-γ (IFNγ) inducing MHC class II expression on various cell types, highlighting these cells' characteristic features (**Supplementary material, Figure S6**). We compared two types of foamy macrophages horizontally and vertically in terms of species and classification. Taking Foamy macrophage in mice and humans as an example, both play a role in the regulation of biological stimulation responses in the BP pathway. However, regardless of species, macrophages with high SPP1 expression actively respond to ficolin-1-rich granule lumen, while macrophages with high TREM2 expression are active in response to oxidative phosphorylation (**Supplementary material, Figure S6**).

In addition, unlike humans, both mouse macrophages exhibit antigen-presenting MHC II-related activation in the CC and MF pathways, while human foamy macrophages

tend to activate the lipid transport pathway. Here, we show only two types of foam cells and inflammatory macrophages. Enrichment analysis of other myeloid cell types is presented in the supplementary material (**Figure 3F-H**) (**Supplementary material, Figure S6**).

It is evident that the myeloid lineages in mouse and humans are conserved, reflecting a common developmental trajectory. Macrophages serve as the origin, differentiating into inflammatory and foamy types. Pseudo-temporal analysis, retaining characteristic genes, identified 20 genes differentially expressed across macrophage types (with mouse genes converted). Late-stage development in foamy macrophages, for instance, is marked by increased expression of genes like TREM2, SPP1, C1QB, and APOC1. In contrast, genes indicative of inflammatory macrophages, such as CCL3, CCL4, and CD74, are upregulated during mid-stage development, whereas TRM-markers trend downwards (**Figure 3I**).

3.5 Inflammatory Signaling and Immune Communication Enhancement Post-AAA.

During the development of abdominal aortic aneurysm (AAA), there is frequently observed immune infiltration by inflammatory cells and the emergence of tertiary lymphoid structures (TLS). To elucidate the mechanisms underlying these observations, we employed CellChat to integrate and compare datasets across different species, thoroughly examining the ligand-receptor interactions among subpopulations within the myeloid cell lineage as well as their interactions with other

529 immune cells (**Figure 4A** and **Figure 4B**). This comprehensive approach aimed to
530 deepen our understanding of the immunological landscape in AAA.
531 Initially, our investigation centered on the interplay between myeloid and global
532 immune cells. Our findings revealed that, relative to controls, both mouse and human
533 specimens demonstrated augmented interactions between inflammatory
534 macrophages (Inf-Mø) and T and B lymphocytes, indicative of an increased
535 recruitment of immune cells. Additionally, the level of communication with fibroblasts
536 was found to be enhanced (**Figure 4A** and **Figure 4B**). Focusing on intra-myeloid cell
537 dynamics, our comparative analysis between AAA and normal conditions across
538 species revealed an augmentation in the activities of foamy macrophages (Foamy-Mø)
539 and macrophages associated with inflammation (ProInf-Mø, Inf-Mø) in AAA (**Figure**
540 **4C, Figure 4D and Figure 4E**). This phenomenon was consistently observed in both
541 mouse and humans, with communication signals between Foamy-Mø and Inf-Mø
542 being notably prominent. Elevated levels of various inflammatory (e.g., IL1, IL16,
543 CD80) and stress-response signals (e.g., THBS, CSF) were detected, underscoring
544 the pathological state. Importantly, TGF-β signaling, which is critical for cell growth and
545 repair and whose receptors play a pivotal role in the arterial wall, was significantly
546 upregulated in the context of AAA (**Figure 4F**).
547 Our multi-layered analysis of the inferred communication networks, leveraging multiple
548 learning and classification techniques, revealed a high expression of osteopontin
549 (SPP1) and amyloidosis-related protein (APP) within Foamy-Mø across both mouse
550 and humans. These findings underscore the conservation of certain cellular

characteristics and functionalities (**Figure 4F**). Delving into the dynamics of ligand-receptor pairs, we observed distinct differences in the cell populations engaged in communication between the disease and control groups. The interaction between Foamy-Mø and Inf-Mø emerged as particularly significant, with the SPP1/CD44 signaling axis notably intensified in AAA in both mouse and humans. Osteopontin (SPP1) facilitates the migration of immune cells, such as macrophages and T cells, by interacting with CD44, thereby participating in the inflammatory response and tissue repair process.

Moreover, our study identified that when foamy macrophages and inflammatory macrophages (Inf-Mø) act as signal senders and receivers, ligands associated with immune cell recruitment (CCL, CXCL) exhibited a pronounced affinity for CCR receptors, a crucial aspect for the mobilization of monocytes, memory T cells, and certain dendritic cell subsets to sites of inflammation or infection. They underscore the intricate interactions between myeloid cells and T, B lymphocytes. Notably, this association is often correlated with the intensity of the immune response. It is noteworthy that individuals with abdominal aortic aneurysm (AAA) exhibit significant activity in chemokine CCL-related pathways, such as CCL3/CCR1 and CCL8/CCR. These pathways facilitate the initiation and maintenance of inflammation by attracting neutrophils and macrophages to the site of inflammation and activating downstream signaling pathways, such as the MAPK/ERK pathway and the PI3K/AKT pathway, which regulate cell proliferation, survival, and differentiation (**Figure 4G**).

Furthermore, Macrophage Migration Inhibitory Factor (MIF) interacts with CD74 and

CD44. MIF exhibits oxidoreductase and chemokine activity and plays a pivotal role in immune and inflammatory responses. Upon binding to CD74 and CD44, it activates multiple signaling pathways, including inflammatory pathways such as MAPK/ERK and PI3K/AKT. Notably, as a ligand sender, MIF may play a role in recruiting immune cells and regulating immune responses (**Figure 4G**). The analysis of these communications, particularly involving foamy and inflammatory macrophages, reveals their critical role in mediating inflammation and amyloidosis, leading to vascular dysfunction in AAA. This phenomenon is evident in both humans and mouse models, facilitated by direct and indirect interactions with immune cells (**Figure 4G**).

The intercellular crosstalk analysis indicates that in AAA, both mice and humans exhibit consistently high expression levels of the ligand SPP1 and the receptor CD44 in myeloid cells. This suggests that AAA promotes inflammation and immune injury by recruiting macrophages to the aneurysm through SPP1/CD44 ligand-receptor interactions. To verify this hypothesis, we performed pathological observations on cross-species AAA tissues. Immunohistochemistry results showed that both SPP1 and CD44 were significantly upregulated in human abdominal aortic aneurysm tissues (*P < 0.05, **P < 0.01) (**Figure 4H, I**). CD44 was predominantly distributed in the macrophages of the intima in arterial tissues, while in AAA, it was extensively distributed in both the intima and adventitia (**Figure 4H**). Similarly, in mouse tissues, specific staining for SPP1 and CD44 was evident in both the adventitia and media (**Figure 4J,K**). Western blotting further demonstrated that the expression level of CD44 in the AAA group was significantly higher than in the control group (**P = 0.0306),

and SPP1 also showed an increasing trend, corroborating the immunohistochemistry results (**Figure 4L**).

3.6 Cross-Species Transcription Factor Analysis in AAA: Unveiling Shared Regulatory Mechanisms.

Moreover, our investigation broadened beyond mere gene-level exploration. Utilizing the SCENIC package, we identified transcription factors shared between human and mouse samples, enabling a comparative analysis of transcriptional activities across species. Within the AAA milieu, we pinpointed 22 transcription factors consistently enriched across both human and mouse specimens (**Figure 5A** and **Figure 5B**). Notably, both TRM and Inf-Mø exhibited concurrent upregulation of Atf3/ATF3 extended, Bclaf1/Bclaf1_extended, and Jund_extended transcription factors in the two species, essential for orchestrating emergency responses and contributing to cellular barrier integrity. Specifically, in IFNIC-Mø, STAT1/STAT1_extended is highly expressed, indicating its critical role in mediating cellular responses to IFN-γ and regulating immune responses, cell proliferation, and apoptosis.

Among other transcription factors, both humans and mouse showed an increasing trend. Transcription factors such as Ets2, FOSB, and Xbp1_extended, highly expressed in Monocytes and ProInf-Mø, are tasked with regulating genes pivotal for cell proliferation and differentiation, as well as engaging in stress responses and endoplasmic reticulum stress mechanisms.NR1H3, predominantly found in the Foamy-Mø cluster, is instrumental in lipid metabolism and cholesterol homeostasis,

playing a vital role in cardiovascular health and inflammatory response modulation, particularly relevant in AAA scenarios characterized by lipid metabolic disruptions and anti-inflammatory activities. Furthermore, MAF/Maf_extended and its variants, by engaging in oxidative stress and inflammatory response pathways, are enriched in Inf-Mø across both humans and mouse (**Figure 5C**). In mouse models, macrophages associated with inflammation-such as IFNIC-Mø, ProInf-Mø, and Inf-Mø—demonstrated shared transcriptional activity of Cebpb/Cebpb extended. Conversely, in human tissues, this transcriptional synergy was predominantly observed in Foamy-Mø, ProInf-Mø, and Monocytes. These transcription factors play crucial roles in cell proliferation, differentiation, and immunological response regulation, notably influencing adipocyte differentiation and the acute phase response.

Irf8_extended showed active transcription in mouse samples, especially within cDC1 cells, underscoring the genetic homology between humans and mouse. Concurrently, pro-inflammatory macrophages exhibited enrichment for NFKB1/NFKB1_extended and Fosb_extended. The transcription factors Crem/crem extend and Rel/Rel_extended (**Figure 5D**), shared by DC1 and DC2, are implicated in cell survival pathways and, as part of the NF-κB family, are instrumental in modulating inflammatory responses and immune regulation. The activation of REL is likely pivotal for the development of the inflammatory milieu and the advancement of pathological processes in AAA.

We selected transcription factors NFKB1 (p50) and STAT1, which are closely related to the SPP1/CD44 ligand-receptor pair and are co-expressed across species. Studies

have shown that STAT1 can be activated through the interferon (IFN)-mediated JAK-STAT pathway, leading to the phosphorylation of STAT1. The activated STAT1 dimers translocate to the nucleus and bind to the promoter region of the CD44 gene, regulating its expression (Stark and Darnell, 2012). Similarly, NFKB1 can activate gene expression by binding to the promoter regions of both SPP1 and CD44. Crosstalk between the STAT1, NFKB1, and SPP1/CD44 pathways has been shown to drive inflammation and immune suppression. To validate this hypothesis, we first examined the expression levels of NFKB1 (p50) and STAT1 in tissues. Immunohistochemistry results showed consistent high expression of NFKB1 (*P = 0.0450) and STAT1 (**P = 0.0332) in human AAA tissues (**Figure 5E,F**). These transcription factors were predominantly localized in the adventitia and media, mirroring the specific distribution pattern of SPP1/CD44. Similarly, extensive specific staining was observed in mouse abdominal aortic aneurysm tissues (**Figure 5G,H**). Western blotting results further confirmed that STAT1 (*P = 0.0238) and NFKB1 (*P = 0.0476) were significantly overexpressed in the AAA group compared to the control group (**Figure 5L**). These experiments suggest that crosstalk between transcription factors and the SPP1/CD44 ligand-receptor pair is a crucial factor in the development of abdominal aortic aneurysms.

4. Discussion

In the present study, we elucidate the intricate complexity and dynamic interplay of cellular constituents in the pathology of abdominal aortic aneurysm (AAA) across

species. A salient finding is the marked dominance of myeloid lineage cells within both human and mouse samples. Delineating cells by employing human ("CD14", "CD68", "LYZ") and mouse ("Adgre1", "Cd68", "Cd14") myeloid lineage-specific markers, we uncovered the identities within these elaborate cellular assemblies. Although the abundance of cells appears consistent, the distinctions between control and disease cohorts demand further exploration(Woollard and Geissmann, 2010). However, our exhaustive scRNA-seq analysis delineates a consistent post-AAA development trend in both humans and mouse: a diminution in SMC content accompanied by a heightened proportion of fibroblasts, indicative of a pathophysiological shift. Moreover, we observed an escalation in immune-related cells (T, B, and myeloid cells), representing a significant departure from the control group.

Cross-species examinations further clarify the pivotal role of myeloid cells in AAA, unveiling an augmentation in fibroblast proportions and immune-related cells subsequent to AAA onset. This alteration, alongside the observed amplification of inflammatory signaling and fortified intercellular communication within myeloid cells, underscores the inflammatory milieu as pivotal in facilitating AAA progression(Van der Borght et al., 2018). Throughout AAA processing, an accretion of foamy macrophages and inflammatory cells is evident, implicating not merely an infiltration by inflammatory cells but also a local metabolic dysregulation and stress in macrophages as contributory to lesion development(Duan et al., 2022). Our research has discovered a matching trend between cross-species and the expression of relevant transcription factors, providing insights into the evolutionary dynamics in AAA pathology.

Additionally, through meticulous single-cell RNA sequencing analysis of human and mouse myeloid cells, we observed that:

1. Integrating data across species, myeloid cells exhibit a high degree of functional overlap and distribution, with macrophage conservation and heterogeneity extending across species boundaries.

2. Cross-species data amalgamation elucidated macrophage types common to humans and mouse, establishing marker genes co-expressed in myeloid cells. It was ascertained that the transcriptional functionality of humans and mouse is largely conserved, with cells of identical classifications demonstrating only nuanced differences in gene functional enrichment and transcription factor activation. 3. Pathological and molecular biology experiments have verified the common expression of matching transcription factors in the cross-species analysis.

Our investigation underscores striking parallels in macrophage subset expression between humans and mouse, emphasizing the conservation of cellular responses in AAA pathology. This finding is pivotal, affirming the validity of mouse models in deciphering human disease mechanisms and in the formulation of targeted gene therapies. Notably, our delineation of specific macrophage subsets, including inflammatory macrophages, tissue-resident macrophages, foamy macrophages, and IFNIC macrophages, may illuminate their roles in disease progression and their therapeutic potential. Through the analysis of intercellular communication, we elucidated specific macrophage subsets and exhibiting species congruence, and confirmed the effectiveness of the prediction in the experiment. Moreover, transcription

factor analysis unveiled common regulatory mechanisms across species, pinpointing key transcription factors potentially governing cellular responses to AAA. This dimension of our study not only deepens our comprehension of the molecular underpinnings but also opens pathways for identifying novel therapeutic targets aimed at altering specific transcriptional activities.

However, although our research results emphasize the complexity of AAA pathology, we lack the in -depth mechanism discussion between transcription factors and compatibility. Future research should aim to clarify the mechanisms behind the dynamic changes in cell populations and their impact on AAA progression. Additionally, exploring targeted intervention measures to regulate different macrophages or transcriptional regulatory factors presents a promising treatment path.

Overall, we have provided valuable insights into the conservativeness of the disease mechanisms through cross-species exploration of AAA cells and transcriptional landscapes, and highlighted the potential of targeted gene therapy. By revealing the complex interactions between cellular entities and regulatory mechanisms, we have laid the foundation for future breakthroughs in the diagnosis, treatment, and prevention of AAA. This underscores the importance of comprehensive research across human and mouse models.

Nevertheless, our findings also accentuate the complexity inherent in AAA pathology, characterized by significant cellular heterogeneity and the complex interrelations among diverse cell types. While our study lays a foundational understanding of the cross-species cellular landscape of AAA, it also underscores the imperative for

subsequent investigations to delve deeper into the specific functions and interactions of these varied cell populations. Future research should endeavor to elucidate the mechanisms underpinning the dynamic shifts in cell populations observed and their influence on AAA progression. Moreover, the exploration of targeted interventions aimed at modulating distinct macrophage subsets or transcriptional regulators emerges as a promising therapeutic avenue. Collectively, our cross-species exploration of the cellular and transcriptional landscape in AAA furnishes valuable insights into the conserved nature of disease mechanisms, spotlighting the potential for targeted gene therapy. By revealing the complex interplays between cellular entities and regulatory mechanisms, we lay the groundwork for future breakthroughs in the diagnosis, treatment, and prevention of AAA, highlighting the significance of integrative human and mouse model studies in translational research.

5. Acknowledgments

Xiaoxu Zhang and Xu Guo contributed equally to this work. Xu Guo mainly responsible for data analysis. Han Jiang was responsible for data collection. Jian Zhang also supervised the project, provided critical revisions, and guided the overall manuscript preparation. Jamol Uzokov, Azad Hussain, Deying Jiang, Yuemeng Li, and Chen Chen provided guidance and support throughout the study. Yanshuo Han and Jian Zhang supervised the project and provided critical revisions. All authors read and approved the final manuscript.

6. Source of Funding

This work was supported by the Fundamental Research Funds for the Central University (Grant No: DUT22YG107), the China Postdoctoral Science (Grant No: 2018M640270), and the Natural Science Foundation of Liaoning Province (Grant No: 2023-MS-096) for Yanshuo Han. Also supported by National Natural Science Foundation of China for Jian Zhang (grant number: 81970402 and 82170507), and International Science and Technology Cooperation Program of Liaoning Province (grant number: 2023JH2/10700019) for Han Jiang.

7. Declarations

Ethics approval and consent to participate

This study was performed according to the Guidelines of the World Medical Association Declaration of Helsinki and was approved by the local ethics committee of the China Medical University. Ethical approval for the study was obtained from the Ethics Committee of the First Hospital of China Medical University (ethical approval number: [2021]134).

Consent for publication

This manuscript contains individual person’s data. Informed written consent was obtained from all participants prior to their inclusion in the study.

Availability of data and materials

Complete single-cell sequencing files of human tissues have been uploaded to the NCBI platform. For mouse datasets, the single-cell sequencing was derived from the

publicly available GEO dataset.

Competing interests

No conflict of interest.

Disclosures

Complete single-cell sequencing files of human tissues have been uploaded to the NCBI platform. For mouse datasets, the single-cell sequencing was derived from the publicly available GEO dataset.

This study does not include any observational research components and did not involve the collection of patient data or samples. Therefore, the STROBE (Strengthening the Reporting of Observational Studies in Epidemiology) guidelines are not applicable to this manuscript.

Conflict of interest

Not Conflict of interest

8. References

Aibar, S., González-Blas, C.B., Moerman, T., Huynh-Thu, V.A., Imrichova, H., Hulselmans, G., Rambow, F., Marine, J.C., Geurts, P., Aerts, J., *et al.* (2017). SCENIC: single-cell regulatory network inference and clustering. Nature methods *14*, 1083-1086.

Aran, D., Looney, A.P., Liu, L., Wu, E., Fong, V., Hsu, A., Chak, S., Naikawadi, R.P., Wolters, P.J., Abate, A.R., *et al.* (2019). Reference-based analysis of lung single-cell sequencing reveals a transitional profibrotic macrophage. Nature Immunology *20*, 163-172.

Bian, Z., Gong, Y., Huang, T., Lee, C.Z.W., Bian, L., Bai, Z., Shi, H., Zeng, Y., Liu, C., He, J., *et al.* (2020). Deciphering human macrophage development at single-cell resolution. Nature *582*, 571-576.

Cao, J., Spielmann, M., Qiu, X., Huang, X., Ibrahim, D.M., Hill, A.J., Zhang, F., Mundlos, S., Christiansen, L., Steemers, F.J., *et al.* (2019). The single-cell transcriptional landscape of mammalian organogenesis. Nature *566*, 496-502.

Clarke, Z.A., Andrews, T.S., Atif, J., Pouyabahar, D., Innes, B.T., MacParland, S.A., and Bader, G.D. (2021). Tutorial: guidelines for annotating single-cell transcriptomic maps using automated and manual methods. Nature Protocols *16*, 2749-2764.

Davis, F.M., Tsoi, L.C., Ma, F., Wasikowski, R., Moore, B.B., Kunkel, S.L., Gudjonsson, J.E., and Gallagher, K.A. (2022). Single-cell Transcriptomics Reveals Dynamic Role of Smooth Muscle Cells and Enrichment of Immune Cell Subsets in Human Abdominal Aortic Aneurysms. Annals of surgery *276*, 511-521.

Duan, Y., Gong, K., Xu, S., Zhang, F., Meng, X., and Han, J. (2022). Regulation of cholesterol homeostasis in health and diseases: from mechanisms to targeted therapeutics. Signal transduction and targeted therapy *7*, 265.

Eming, S.A., Wynn, T.A., and Martin, P. (2017). Inflammation and metabolism in tissue repair and regeneration. Science (New York, N.Y.) *356*, 1026-1030.

Gao, J., Cao, H., Hu, G., Wu, Y., Xu, Y., Cui, H., Lu, H.S., and Zheng, L. (2023). The mechanism and therapy of aortic aneurysms. Signal transduction and targeted therapy *8*, 55.

Golledge, J. (2019). Abdominal aortic aneurysm: update on pathogenesis and medical treatments. Nature reviews. Cardiology *16*, 225-242.

Han, J., Gallerand, A., Erlich, E.C., Helmink, B.A., Mair, I., Li, X., Eckhouse, S.R., Dimou, F.M., Shakhsheer, B.A., Phelps, H.M., *et al.* (2024). Human serous cavity macrophages and dendritic cells possess counterparts in the mouse with a distinct distribution between species. Nature immunology *25*, 155-165.

Ishibashi, M., Egashira, K., Zhao, Q., Hiasa, K., Ohtani, K., Ihara, Y., Charo, I.F., Kura, S., Tsuzuki, T., Takeshita,

A., *et al.* (2004). Bone marrow-derived monocyte chemoattractant protein-1 receptor CCR2 is critical in angiotensin II-induced acceleration of atherosclerosis and aneurysm formation in hypercholesterolemic mice. Arteriosclerosis, thrombosis, and vascular biology *24*, e174-178.

Jin, S., Guerrero-Juarez, C.F., Zhang, L., Chang, I., Ramos, R., Kuan, C.-H., Myung, P., Plikus, M.V., and Nie, Q. (2021). Inference and analysis of cell-cell communication using CellChat. Nature Communications *12*, 1088.

Korsunsky, I., Millard, N., Fan, J., Slowikowski, K., Zhang, F., Wei, K., Baglaenko, Y., Brenner, M., Loh, P.-r., and Raychaudhuri, S. (2019). Fast, sensitive and accurate integration of single-cell data with Harmony. Nature Methods *16*, 1289-1296.

McGinnis, C.S., Murrow, L.M., and Gartner, Z.J. (2018). DoubletFinder: Doublet detection in single-cell RNA sequencing data using artificial nearest neighbors. bioRxiv, 352484.

Murray, P.J., Allen, J.E., Biswas, S.K., Fisher, E.A., Gilroy, D.W., Goerdt, S., Gordon, S., Hamilton, J.A., Ivashkiv, L.B., Lawrence, T., *et al.* (2014). Macrophage activation and polarization: nomenclature and experimental guidelines. Immunity *41*, 14-20.

Nahrendorf, M., and Swirski, F.K. (2016). Abandoning M1/M2 for a Network Model of Macrophage Function. Circulation research *119*, 414-417.

Nalio Ramos, R., Missolo-Koussou, Y., Gerber-Ferder, Y., Bromley, C.P., Bugatti, M., Núñez, N.G., Tosello Boari, J., Richer, W., Menger, L., Denizeau, J., *et al.* (2022). Tissue-resident FOLR2(+) macrophages associate with CD8(+) T cell infiltration in human breast cancer. Cell *185*, 1189-1207.e1125.

Nordon, I.M., Hinchliffe, R.J., Loftus, I.M., and Thompson, M.M. (2011). Pathophysiology and epidemiology of abdominal aortic aneurysms. Nature reviews. Cardiology *8*, 92-102.

Orecchioni, M., Ghosheh, Y., Pramod, A.B., and Ley, K. (2019). Macrophage Polarization: Different Gene Signatures in M1(LPS+) vs. Classically and M2(LPS-) vs. Alternatively Activated Macrophages. Frontiers in immunology *10*, 1084.

Ouyang, Y., Hong, Y., Mai, C., Yang, H., Wu, Z., Gao, X., Zeng, W., Deng, X., Liu, B., Zhang, Y., *et al.* (2024). Transcriptome analysis reveals therapeutic potential of NAMPT in protecting against abdominal aortic aneurysm in human and mouse. Bioactive materials *34*, 17-36.

Qiu, X., Hill, A., Packer, J., Lin, D., Ma, Y.-A., and Trapnell, C. (2017a). Single-cell mRNA quantification and differential analysis with Census. Nature Methods *14*, 309-315.

Qiu, X., Mao, Q., Tang, Y., Wang, L., Chawla, R., Pliner, H.A., and Trapnell, C. (2017b). Reversed graph embedding resolves complex single-cell trajectories. Nature Methods *14*, 979-982.

Raffort, J., Lareyre, F., Clément, M., Hassen-Khodja, R., Chinetti, G., and Mallat, Z. (2017). Monocytes and macrophages in abdominal aortic aneurysm. Nature Reviews Cardiology *14*, 457-471.

Rateri, D.L., Howatt, D.A., Moorleghen, J.J., Charnigo, R., Cassis, L.A., and Daugherty, A. (2011). Prolonged infusion of angiotensin II in apoE(-/-) mice promotes macrophage recruitment with continued expansion of abdominal aortic aneurysm. The American journal of pathology *179*, 1542-1548.

Sakalihasan, N., Limet, R., and Defawe, O.D. (2005). Abdominal aortic aneurysm. Lancet (London, England) *365*, 1577-1589.

Sakalihasan, N., Michel, J.-B., Katsargyris, A., Kuivaniemi, H., Defraigne, J.-O., Nchimi, A., Powell, J.T., Yoshimura, K., and Hultgren, R. (2018). Abdominal aortic aneurysms. Nature Reviews Disease Primers *4*, 34.

Sawada, H., Lu, H.S., and Daugherty, A. (2021). Single-cell transcriptomics as a building block for determining mechanistic insight of abdominal aortic aneurysm formation. Cardiovascular research *117*, 1243-1244.

Shi, Y., Zhang, Q., Bi, H., Lu, M., Tan, Y., Zou, D., Ge, L., Chen, Z., Liu, C., Ci, W., *et al.* (2022). Decoding the

multicellular ecosystem of vena caval tumor thrombus in clear cell renal cell carcinoma by single-cell RNA sequencing. Genome biology *23*, 87.
Stark, G.R., and Darnell, J.E., Jr. (2012). The JAK-STAT pathway at twenty. Immunity *36*, 503-514.
Stuart, T., Butler, A., Hoffman, P., Hafemeister, C., Papalexi, E., Mauck, W.M., 3rd, Hao, Y., Stoeckius, M., Smibert, P., and Satija, R. (2019). Comprehensive Integration of Single-Cell Data. Cell *177*, 1888-1902.e1821.
Trapnell, C., Cacchiarelli, D., Grimsby, J., Pokharel, P., Li, S., Morse, M., Lennon, N.J., Livak, K.J., Mikkelsen, T.S., and Rinn, J.L. (2014). The dynamics and regulators of cell fate decisions are revealed by pseudotemporal ordering of single cells. Nature Biotechnology *32*, 381-386.
Trollope, A., Moxon, J.V., Moran, C.S., and Golledge, J. (2011). Animal models of abdominal aortic aneurysm and their role in furthering management of human disease. Cardiovascular pathology : the official journal of the Society for Cardiovascular Pathology *20*, 114-123.
Van der Borght, K., Scott, C.L., Martens, L., Sichien, D., Van Isterdael, G., Nindl, V., Saeys, Y., Boon, L., Ludewig, B., Gillebert, T.C.*, et al.* (2018). Myocarditis Elicits Dendritic Cell and Monocyte Infiltration in the Heart and Self-Antigen Presentation by Conventional Type 2 Dendritic Cells. Frontiers in immunology *9*, 2714.
Woollard, K.J., and Geissmann, F. (2010). Monocytes in atherosclerosis: subsets and functions. Nature reviews. Cardiology *7*, 77-86.
Yang, J., Zhang, L., Yu, C., Yang, X.F., and Wang, H. (2014). Monocyte and macrophage differentiation: circulation inflammatory monocyte as biomarker for inflammatory diseases. Biomarker research *2*, 1.
Yu, G., Wang, L.-G., Han, Y., and He, Q.-Y. (2012). clusterProfiler: an R Package for Comparing Biological Themes Among Gene Clusters. OMICS: A Journal of Integrative Biology *16*, 284-287.
Yu, L., Zhang, J., Gao, A., Zhang, M., Wang, Z., Yu, F., Guo, X., Su, G., Zhang, Y., Zhang, M.*, et al.* (2022). An intersegmental single-cell profile reveals aortic heterogeneity and identifies a novel Malat1(+) vascular smooth muscle subtype involved in abdominal aortic aneurysm formation. Signal transduction and targeted therapy *7*, 125.
Zernecke, A., Erhard, F., Weinberger, T., Schulz, C., Ley, K., Saliba, A.E., and Cochain, C. (2023). Integrated single-cell analysis-based classification of vascular mononuclear phagocytes in mouse and human atherosclerosis. Cardiovascular research *119*, 1676-1689.
Zhang, K., Wang, Y., Chen, S., Mao, J., Jin, Y., Ye, H., Zhang, Y., Liu, X., Gong, C., Cheng, X.*, et al.* (2023). TREM2(hi) resident macrophages protect the septic heart by maintaining cardiomyocyte homeostasis. Nature metabolism *5*, 129-146.
Zhao, G., Lu, H., Chang, Z., Zhao, Y., Zhu, T., Chang, L., Guo, Y., Garcia-Barrio, M.T., Chen, Y.E., and Zhang, J. (2021). Single-cell RNA sequencing reveals the cellular heterogeneity of aneurysmal infrarenal abdominal aorta. Cardiovascular research *117*, 1402-1416.

9. Figure Legends

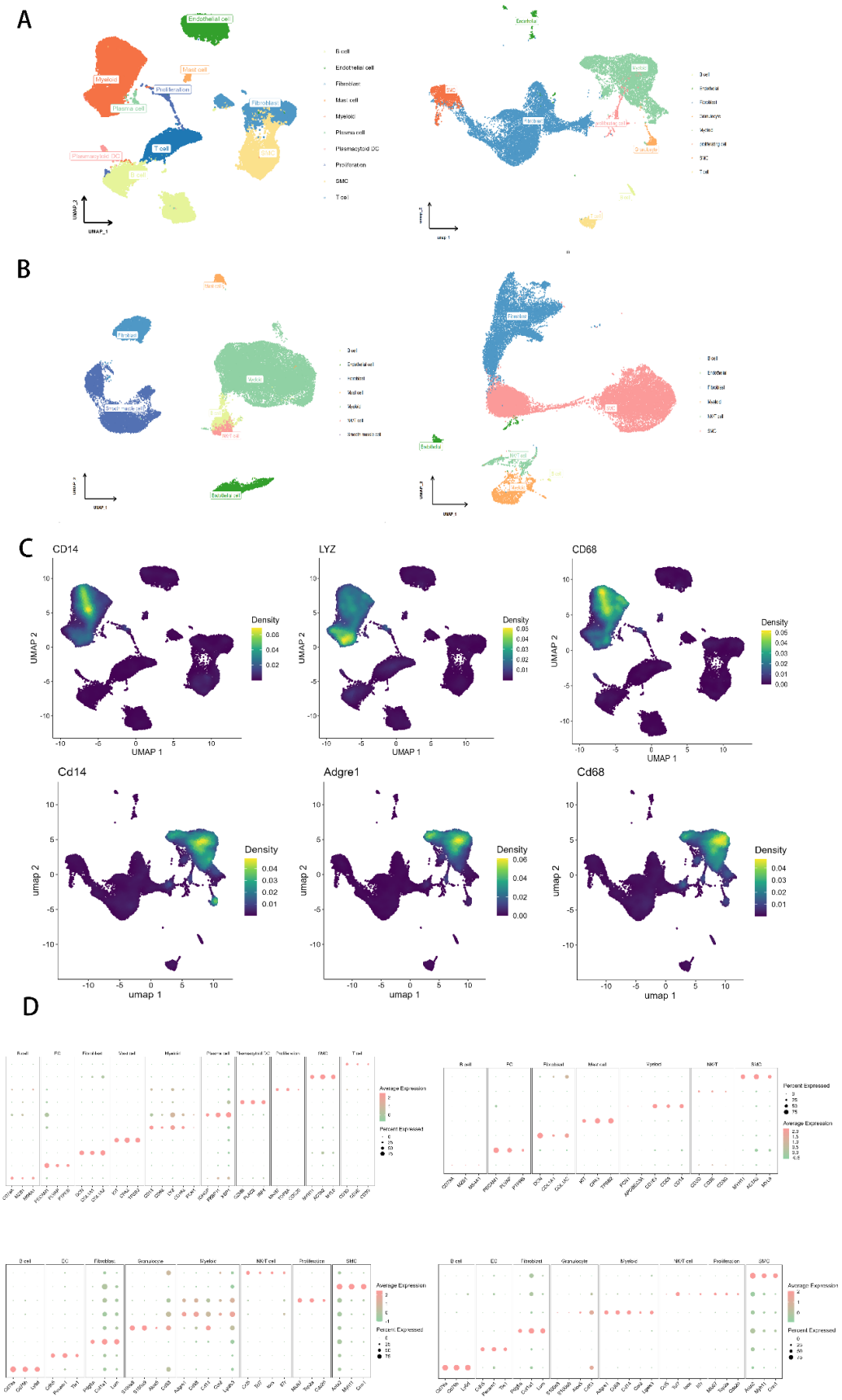

Figure 1. Presents the results of single-cell sequencing dimensionality reduction for

abdominal aortic aneurysm (AAA) in humans and mice. **A**. After unsupervised clustering, Uniform Manifold Approximation and Projection (UMAP) visualizations are provided for 7 human AAA tissues (left) and 7 mouse AAA tissues (right). Each point represents an individual cell, colored according to cluster designation. **B**. UMAP dimensionality reduction results for 6 normal human (left) and 4 normal mouse tissues(right). **C**. UMAP projection of biologically significant marker genes in human and mouse AAA tissues. **D**. The DotPlot illustrates the distribution and expression of specific marker genes across each cell population, highlighting the distinctive biological markers associated with each. The plot includes data from both human and mouse tissues, with human tissue samples (AAA n=7, control n=6) on the left and mouse tissue samples (AAA n=7, control n=4) on the right. The top section represents AAA samples, while the bottom section represents normal samples. (Human tissue, AAA n=7 control n=6. Mouse tissue, AAA n=7 control n=4.)

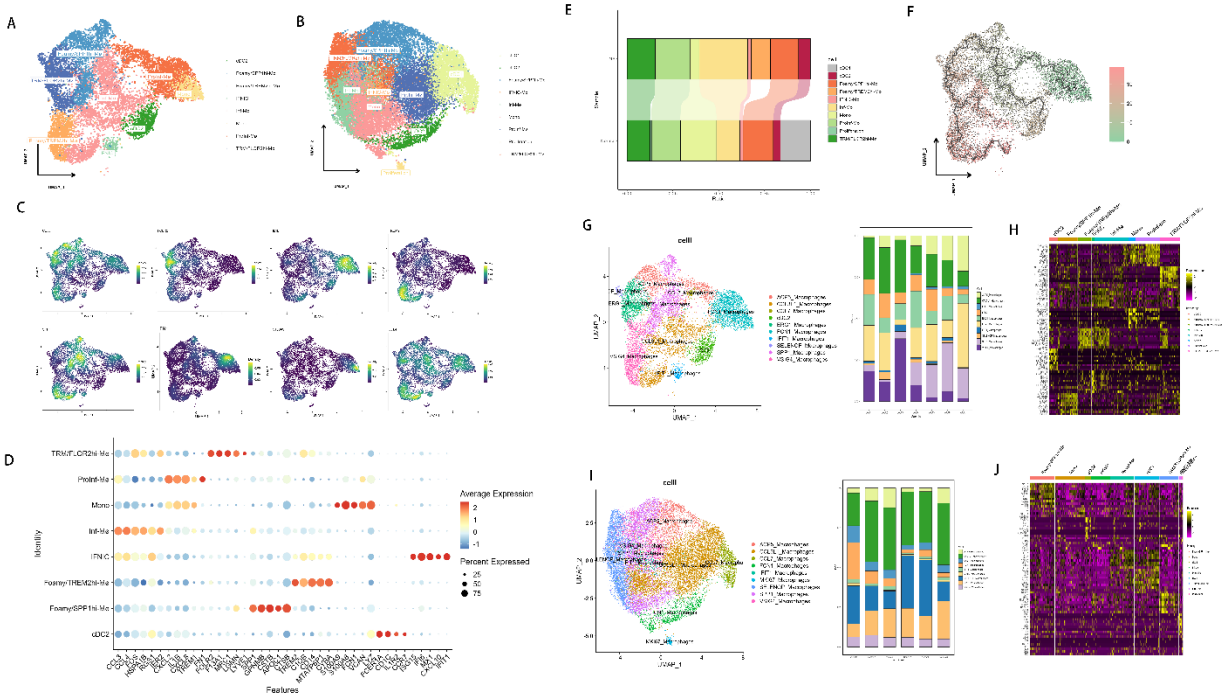

Figure 2. Comprehensive Single-Cell RNA Sequencing Analysis of Human Myeloid Cells in Abdominal Aortic Aneurysm. **A**. UMAP visualization illustrates the dimensional reduction and clustering of 10,793 myeloid cells derived from patients with abdominal aortic aneurysm **B**. UMAP dimensionality reduction results for 21,172 normal human cells **C**. Identification of specific marker genes for each myeloid cell subgroup, with their distribution across clusters visualized on the UMAP plots, facilitating a detailed examination of gene expression landscapes. **D**. A DotPlot representation highlights the six most prominently expressed genes within each cluster, offering insights into the differential gene expression profiles characteristic of each identified cell population. **E**. The columnar Sankey plot reflects the proportion of human cells between the disease group and the normal group. **F**. Pseudotime analysis of the myeloid cell trajectories illuminates temporal expression trends and developmental pathways within the myeloid cell compartment, suggesting potential progression patterns in the context of abdominal aortic aneurysm pathogenesis. **G**. In human abdominal aortic

aneurysm (AAA) samples, the classification of human myeloid cell lines based on genes with specific biological functions and their proportional distribution across samples. **H.** Heatmap showing the proportion of different cell types within myeloid cells from human AAA samples. **I.** In normal human aortic samples, the classification of human myeloid cell lines based on genes with specific biological functions and their proportional distribution across samples. **J.** Heatmap showing the proportion of different cell types within myeloid cells from normal human aortic samples.(Human tissue, AAA n=7 control n=6.)

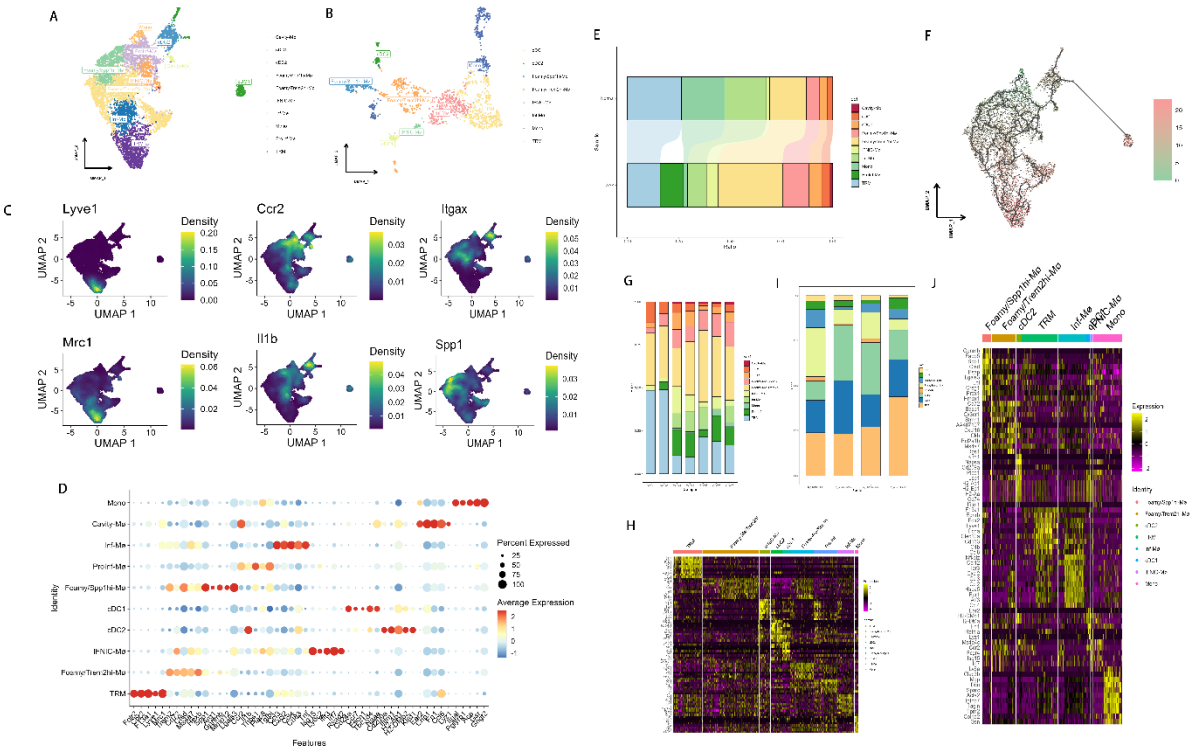

965

966 **Figure 3**. Comprehensive Single-Cell RNA Sequencing Analysis of Mouse Myeloid
967 Cells in Abdominal Aortic Aneurysm. **A.** The UMAP visualization depicts the
968 dimensionality reduction and clustering of myeloid cell populations harvested from
969 mouse models (6,521 cells) of abdominal aortic aneurysm. **B.** Comparative
970 dimensionality reduction and clustering analysis results for 4 normal mouse aortic
971 samples. **C.** Systematic identification and UMAP projection of specific marker genes
972 for each myeloid cell subgroup, thereby enabling a comprehensive exploration of gene
973 expression patterns across different clusters in mouse AAA. **D.** A DotPlot visual
974 underscores the top six genes exhibiting the highest expression levels within each
975 cluster, shedding light on the unique gene expression signatures prevalent among the
976 various myeloid cell populations in mouse AAA. **E.** A columnar Sankey diagram
977 delineates the cellular composition disparities between the diseased and normal
978 cohorts, quantitatively illustrating the cell distribution shifts attributable to the

pathological state. **F.** Pseudotemporal ordering of myeloid cells unveils the evolutionary expression trends and delineates the developmental trajectories within the myeloid compartment, elucidating the potential mechanistic pathways implicated in the progression of abdominal aortic aneurysm in mouse models. **G.** The proportional distribution of various myeloid cell components in different samples from mice with AAA. **H.** Gene heatmap, where yellow highlights indicate high gene expression in a specific cell type. **I.** Proportional distribution of myeloid cells in normal mouse aortic samples. **J.** Heatmap showing the distribution of different myeloid cell components in normal mouse aortic samples. (Mouse tissue, AAA n=7 control n=4.)

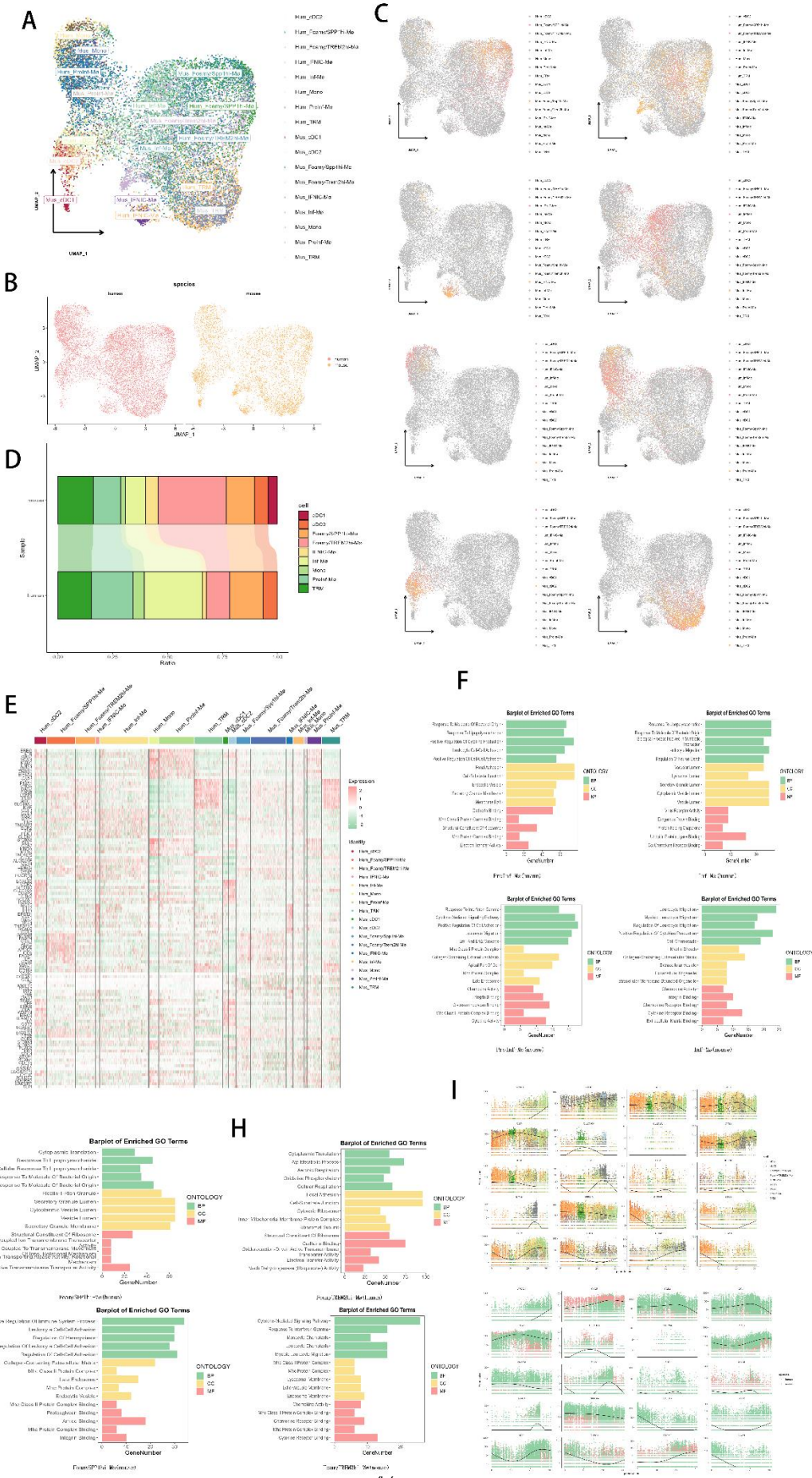
A
B
species
human
mouse
C
D
Sample
Ratio
cell
E
F
Barplot of Enriched GO Terms
GeneNumber
ONTOLOGY
BP
CC
MF
G
H
I

Figure 3. Integrated Analysis of scRNA-seq Data on Macrophages from Mouse and Human Abdominal Aortic Aneurysms Across Species. **A.** Results of UMAP dimensionality reduction before and after translating to human gene symbols reveal 16,314 cells, illustrating the comparative genomics approach. **B.** Cross-species distribution plots for human and mouse data are differentiated by color coding, facilitating direct visual comparison. Red represents human cells, while yellow represents mouse cells. **C.** UMAP visualization reveals the distribution of macrophage cell types in both mice and humans, showcasing similar spatial distribution patterns across species. **D.** Trends in the proportion of various macrophage types within human and mouse AAA contexts are quantitatively analyzed. **E.** Within the integrated human-mouse cluster, a heatmap of highly expressed genes (selected based on the top 10) enables intuitive comparisons of gene expression differences in identical macrophage types between humans and mice. **F-G-H**. By conserving genes common to both species, the 'FindMarkers' function was utilized to conduct GO enrichment analysis on macrophage subtypes including ProInf-Mø, Inf-Mø, Foamy/SPP1^{hi}-Mø, and Foamy/TREM2^{hi}-Mø, among others. **I**. Pseudo-temporal analysis, initiating with monocytes, elucidates gene expression evolution over pseudo-time. (Human tissue, AAA n=7. Mouse tissue, AAA n=7.)

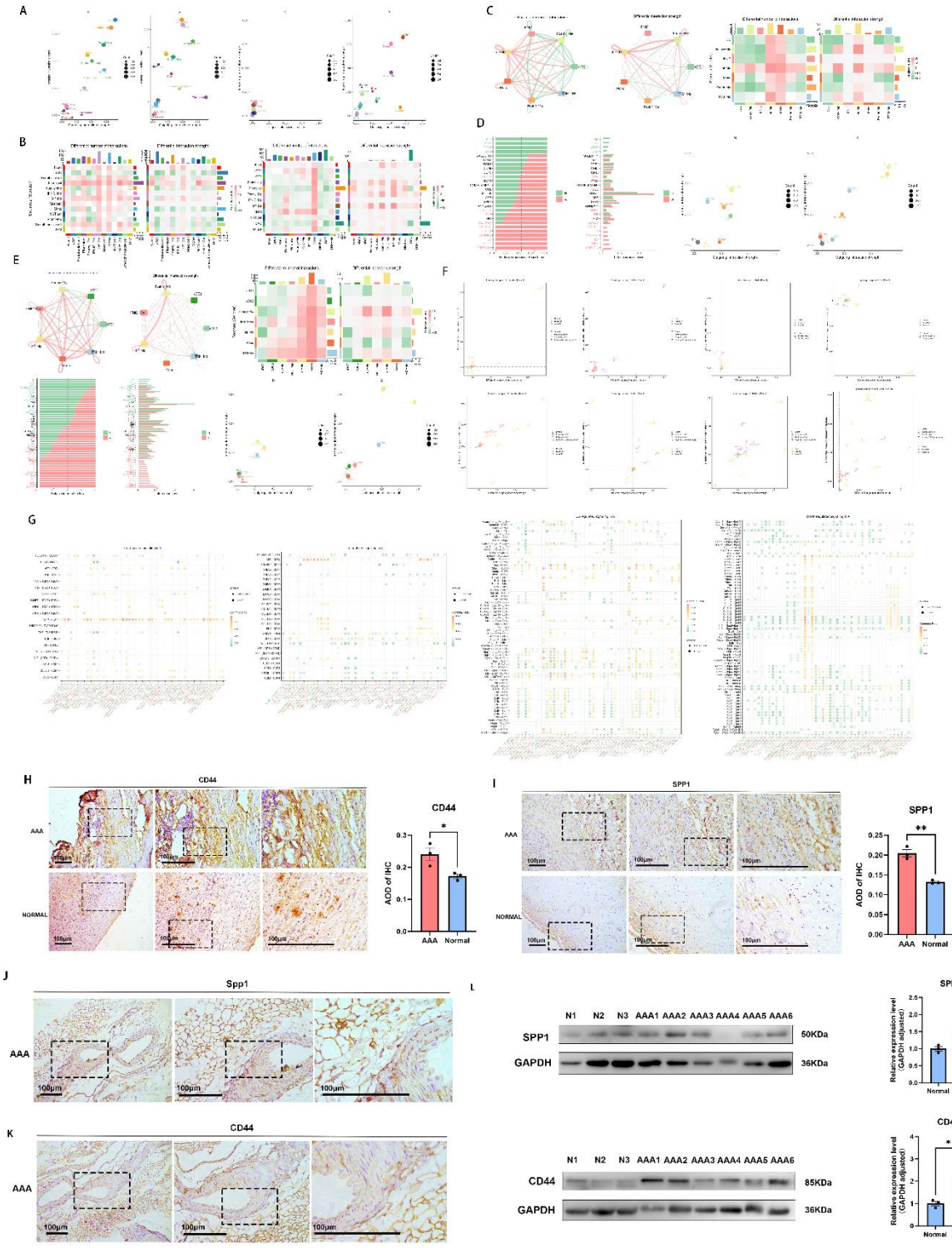

Figure 4. Myeloid Cross-Species Communication and Intra/outra-Myeloid Cellular Dialogues Reveal Homogeneous Complex Signal Transduction in AAA. **A-B.** Communication intensity between myeloid and other cell types is shown for humans (left) and mice (right). This includes 17,314 myeloid cells from abdominal aortic

aneurysm (AAA) and 21,172 myeloid cells from the normal human population. For mice, the data includes 6,440 myeloid cells from AAA and 1,467 myeloid cells from the normal population. **C.** Intra-human myeloid cell communication results, where pink indicates an upregulated trend in communication signals between two cell types in AAA compared to the control group, and green indicates the opposite. **D.** Enrichment of signaling pathways across various classes and genera of macrophages, reflecting the functional role of each class of macrophages in the progression of human AAA. **E.** Intra-mouse myeloid cell communication, exhibiting patterns similar to those observed in humans.Also shows the enrichment of receptor pairs in mouse AAA. **F.** The enrichment of receptor pairs in foamy and inflammatory macrophages active across different species in AAA, with various celltypes. (Above are the communication results for human AAA; below are the communication results for mouse AAA.) **G.** A dot plot shows the changing trend of AAA ligand pairs compared with the control group. Among them, specific ligand pairs show a common up-regulation trend in different species (left: human as both donor and receptor, right: mouse as both donor and receptor, related to inflammation and foam cell macrophages). (Human tissue, AAA n=7 control n=6. Mouse tissue, AAA n=7 control n=4.) **H.** IHC(Immunohistochemical) of control and AAA tissues (magnification ×100, ×200, ×400). Compared to the control group, CD44 expression in human abdominal aortic aneurysm (AAA) tissues is significantly upregulated. **I.** IHC shows that SPP1 (**P = 0.0016) is significantly upregulated in human AAA tissues (magnification ×100, ×200, ×400). **J.** Immunohistochemical of Spp1 in cross-sections of the lumen of mouse AAA tissue, scale bar 100μm. **K.**

Immunohistochemical of CD44 in cross-sections of the lumen of mouse AAA tissue, scale bar 100μm. **L.** Western blot analysis showing the expression of proteins SPP1 (P = 0.1993) and CD44 (**P = 0.0306) in AAA and normal tissues. Data are presented as mean ± SD; (Normal n = 3, AAA n = 6).

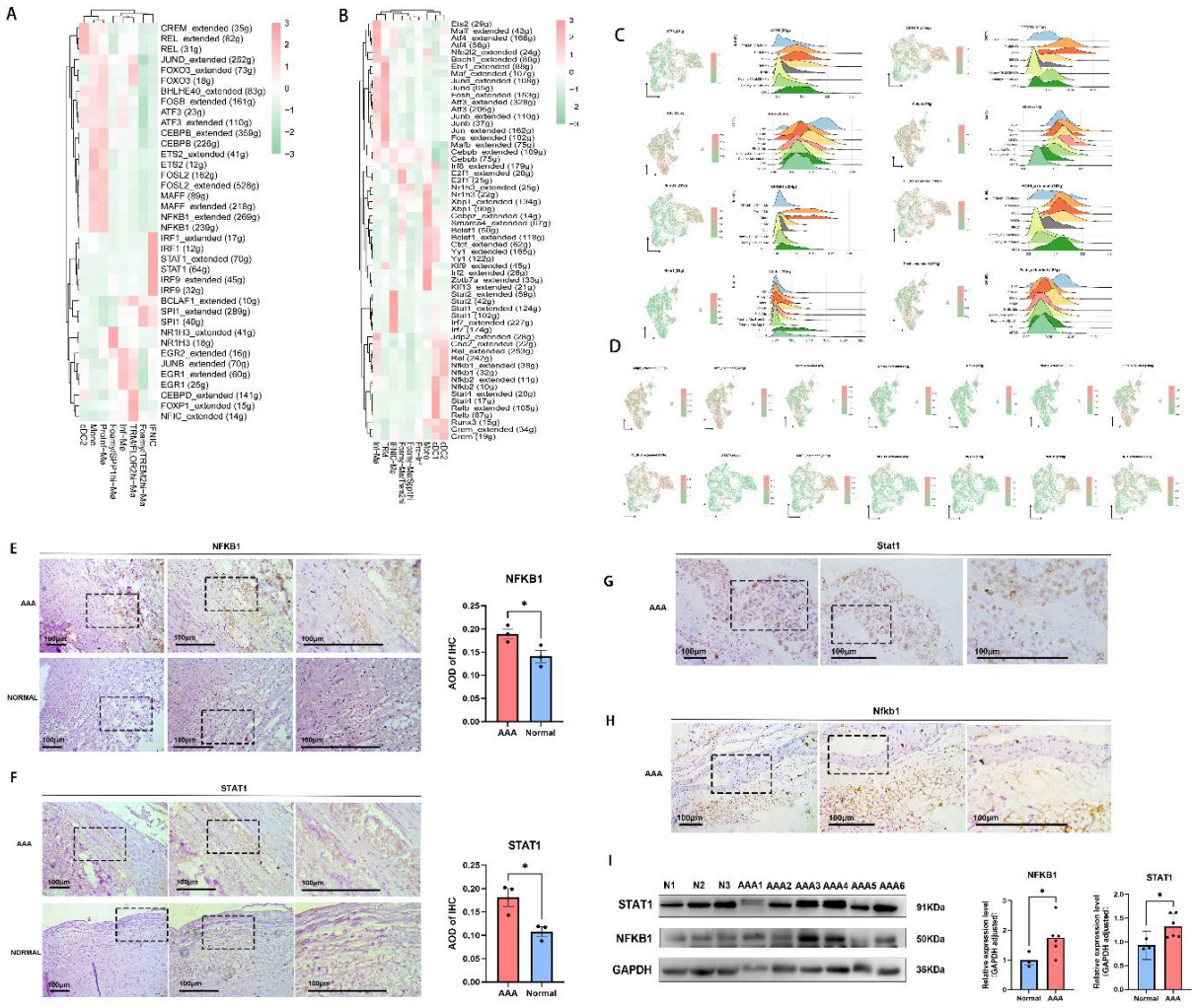

Figure 5. Examination of Cross-Species Transcription Factors. **A.** Utilization of the SCENIC package to investigate the enrichment heatmap of transcription factors in 17,314 human myeloid cells. **B.** Enrichment heatmap of transcription factors in 6,521 mouse myeloid cells. **C.** Comparative analysis of enriched and differentially expressed transcripts in various cell types across human and mouse species. **D.** Visual representation of co-enriched transcription factors in both species. (Human tissue, AAA n=7 .Mouse tissue, AAA n=7). **E.** Immunohistochemical shows the spatial distribution of the transcription factor NFKB1 in human abdominal aortic aneurysm (AAA) tissues. Compared to the control group, NFKB1 expression is significantly upregulated (*P = 0.0332) (magnification ×100, ×200, ×400). **F.** Immunohistochemical

shows the spatial distribution of the transcription factor STAT1 in human AAA tissues. Compared to the control group, STAT1 expression is significantly upregulated (*P = 0.0332) (magnification ×100, ×200, ×400). **G.** Immunohistochemical of Stat1 in cross-sections of the lumen of mouse AAA tissue, scale bar 100μm. **H.** Immunohistochemical of Nfkb1 in cross-sections of the lumen of mouse AAA tissue, scale bar 100μm. **I.** Western blot analysis showing the expression of proteins STAT1 (*P = 0.0238) and NFKB1 (*P = 0.0476) in AAA and normal tissues. Data are presented as mean ± SD; (Normal n = 3, AAA n = 6).